International Journal of Applied Earth Observation and Geoinformation xxx (2010) xxx–xxx

Contents lists available at ScienceDirect

International Journal of Applied Earth Observation and Geoinformation

journal homepage: www.elsevier.com/locate/jag

Monitoring global land surface drought based on a hybrid evapotranspiration model

Yunjun Yao[a,b,c,*], Shunlin Liang[b,c], Qiming Qin[a], Kaicun Wang[b], Shaohua Zhao[a]

[a] Institute of Remote Sensing and GIS, Peking University, Beijing 100871, China
[b] Department of Geography, University of Maryland, College Park, MD 20742, USA
[c] College of Global Change and Earth System Science, Beijing Normal University, Beijing 100875, China

ARTICLE INFO

Article history:
Received 20 May 2010
Accepted 16 September 2010

Keywords:
Global land surface drought
Hybrid ET model
Potential ET
Evaporative Drought Index
Palmer Drought Severity Index

ABSTRACT

The latent heat of evapotranspiration (ET) plays an important role in the assessment of drought severity as one sensitive indicator of land drought status. A simple and accurate method of estimating global ET for the monitoring of global land surface droughts from remote sensing data is essential. The objective of this research is to develop a hybrid ET model by introducing empirical coefficients based on a simple linear two-source land ET model, and to then use this model to calculate the Evaporative Drought Index (EDI) based on the actual estimated ET and the potential ET in order to characterize global surface drought conditions. This is done using the Global Energy and Water Cycle Experiment (GEWEX) Surface Radiation Budget (SRB) products, AVHRR-NDVI products from the Global Inventory Modeling and Mapping Studies (GIMMS) group, and National Centers for Environmental Prediction Reanalysis-2 (NCEP-2) datasets. We randomly divided 22 flux towers into two groups and performed a series of cross-validations using ground measurements collected from the corresponding flux towers. The validation results from the second group of flux towers using the data from the first group for calibration show that the daily bias varies from $-6.72\,W/m^2$ to $12.95\,W/m^2$ and the average monthly bias is $-1.73\,W/m^2$. Similarly, the validation results of the first group of flux towers using data from second group for calibration show that the daily bias varies from $-12.91\,W/m^2$ to $10.26\,W/m^2$ and the average monthly bias is $-3.59\,W/m^2$. To evaluate the reliability of the hybrid ET model on a global scale, we compared the estimated ET from the GEWEX, AVHRR-GIMMS-NDVI, and NECP-2 datasets with the latent heat flux from the Global Soil Wetness Project-2 (GSWP-2) datasets. We found both of them to be in good agreement, which further supports the validity of our model's global ET estimation. Significantly, the patterns of monthly EDI anomalies have a good spatial and temporal correlation with the Palmer Drought Severity Index (PDSI) anomalies from January 1984 to December 2002, which indicates that the method can be used to accurately monitor long-term global land surface drought.

© 2010 Elsevier B.V. All rights reserved.

1. Introduction

Drought is a chronic potential natural disaster characterized by an extended period of time in which less water is available than expected in an ecological system (Ghulam et al., 2007; Robeson, 2008). The Evaporative Drought Index (EDI), which is defined as 1 minus the ratio of actual latent heat of evapotranspiration (ET) to potential ET (PET), is one of the most significant metrics denoting the soil moisture response to surface dryness (Yao et al., 2010). This is because actual ET is a significant process that drives the energy and water exchange between the atmosphere and land surface (Priestley and Taylor, 1972; Wang et al., 2007; Wang and Liang, 2008), and PET is the result of all other driving factors functioning when soil moisture is not limited. Unlike other drought indices, the EDI is easy to calculate and it also integrates the energy radiation, which is an effective operational method for drought monitoring. In a previous study, Yao et al. (2010) applied the EDI to both canopy transpiration and soil evaporation by using a simple empirical ET equation, and obtained good results for surface dryness estimates over the contiguous United States.

Numerous studies have shown that the ratio of ET to PET can be related to soil and plant water potentials (Abramopoulos et al., 1988; Mahfouf and Noilhan, 1991; Song et al., 2000). When a plant has adequate water available it will transpire at the potential ET rate. Similarly, the actual ET rate will fall below the potential ET rate if water is limited (McVicar and Jupp, 1998; Kalma et al., 2008). Therefore, methods for combining the ET and PET have been used extensively for drought monitoring on landscape and regional scales over the last several decades. The Crop Water

* Corresponding author at: Institute of Remote Sensing and GIS, Peking University, Beijing 100871, China. Tel.: +86 10 6276 5715.
E-mail address: boyyunjun@163.com (Y. Yao).

0303-2434/$ – see front matter © 2010 Elsevier B.V. All rights reserved.
doi:10.1016/j.jag.2010.09.009

Stress Index (CWSI) (see Idso et al., 1981; Jackson, 1982) was developed to estimate the full canopy water content using the ratio of actual ET to PET. Subsequently, Choudhury (1983) described the CWSI as the difference between canopy temperature and air temperature. Moran et al. (1994) extended its application to partial canopies to create the Water Deficit Index (WDI) for canopy water estimation (also referred to as the Vegetation Index-Temperature Trapezoid, VITT), by using the Penman–Monteith equation with known values of net radiation, water vapor pressure, and wind speed. Lambin and Ehrlich (1996) also adopted a trapezoid-method similar to that of Moran et al. (1994) to study the water stress of heterogeneous landscapes. Anderson et al. (2007a,b) recently used the Atmosphere-Land Exchange Inverse (ALEXI) model to estimate surface latent heat fluxes and to assess soil moisture across the continental United States, based on the Evaporative Stress Index (ESI). The weakness of these methods for estimating global ET limits and their application to global drought monitoring, however, is that ET is difficult to measure and predict on global spatial scales.

Global ET estimations in the literature have been characterized by the parallel development of complicated realistic models that require complex parameters, and simple empirical models that lack realistic mechanisms (Cleugh et al., 2007; Fisher et al., 2008). In general, more complex physical and analytical methods are not necessarily more accurate than simple statistical or empirical methods, though the datasets required to support some of the empirical methods are not readily available (Kalma et al., 2008). Therefore, the application of a simple empirical ET method is necessary when more detailed input data is not available. In contrast, traditional ET estimation models require numerous physical input parameters, which are not easy to acquire on a global scale. For example, though both the Soil and Water Assessment Tool (SWAT) (Arnold et al., 1998a,b) and Variable Infiltration Capacity (VIC) (Wood et al., 1992) require precipitation data derived from surface gauge networks, satellite imagery or modeling as an input, data on the subsurface soil texture is also needed. Many satellite ET estimation methods, including Two-source Surface Energy Balance (TSEB) (Shuttleworth and Wallace, 1985), Surface Energy Balance Algorithm for Land (SEBAL) (Bastiaanssen et al., 1998a,b), Simplified Surface Energy Balance approach (SSEB) models (Senay et al., 2007), which use the Map ET at high Resolutions with Internal Calibration (METRIC) (Tittebrand et al., 2005; Allen et al., 2007a,b) and the LST/NDVI triangle feature space methods (Gillies et al., 1997; Wang et al., 2006), often suffer from temporal and spatial gaps due to cloud cover and the infrequency of satellite images. Recently, an operational remote sensing algorithm for land surface evaporation based on a simple linear two-source land ET model was developed by Nishida et al. (2003). It has proven to be effective for estimating ET at regional-scale applications using MODIS data. However, it still requires too many input parameters (including wind speed and cuticle resistance) to be of practical use in estimating actual ET. As a result, the ET model will ultimately grow in complexity.

This study has two major objectives. First, based on the above mentioned simple linear two-source land ET model, we introduce a linear combination of the most important parameters (air temperature, net radiation, etc.) controlling the actual ET to simplify the evaporative fraction (EF), and to then develop a new hybrid ET model. We also validate the hybrid ET model using Atmosphere Radiation Measurement (ARM), FLUXNET and data from Chinese experiments. Second, we use the EDI to infer global land surface dryness conditions from 1984 to 2002 using the hybrid ET model with GEWEX, AVHRR-GIMMS-NDVI, and NCEP-2 products. The EDI patterns are compared with Palmer Drought Severity Index (PDSI) products to determine the validity of the method's drought assessment on a global scale.

2. Data and methodology

2.1. Data

We used global monthly surface downward and upward shortwave and longwave radiation products at a spatial resolution of $1^\circ \times 1^\circ$ from 1984 to 2002 that were derived from the Global Energy and Water Cycle Experiment (GEWEX) Surface Radiation Budget (SRB) products (http://gewex-srb.larc.nasa.gov/common/php/SRB_data_products.php). The monthly NDVI at a 1-degree spatial resolution is from the Global Inventory Modeling and Mapping Studies (GIMMS) group at the National Aeronautics and Space Administration (NASA) Goddard Space Flight Center (Tucker et al., 2005), which was obtained from National Oceanic and Atmospheric Administration (NOAA)/AVHRR observations (http://islscp2.sesda.com/ISLSCP2_1/data/vegetation/gimms_ndvi_monthly _xdeg/). The monthly air mean temperature, and the maximum and minimum air temperature data were extracted from the National Centers for Environmental Prediction Reanalysis-2 (NCEP-2) data, which were acquired from the NCEP/NCAR Reanalysis Project (CDAS). These data (downloaded from http://www.cpc.ncep.noaa.gov/products/wesley/reanalysis.html) are found on the T-62 Gaussian grid, which has a spatial resolution of 1.875° longitude by approximately 1.9° latitude, and are interpolated into $1^\circ \times 1^\circ$ using bilinear interpolation.

To design and evaluate the hybrid ET model, MODIS NDVI composite products with a 1-km spatial resolution and a 16-day temporal resolution were used (downloaded from https://wist.echo.nasa.gov/api/). The daily NDVI values were temporally interpolated from the 16-day averages using linear interpolation. We also used the flux data from twelve Atmospheric Radiation Measurement (ARM) towers (EF02, EF04, EF07, EF08, EF09, EF12, EF13, EF15, EF18, EF19, EF20, and EF26) (downloaded from http://www.archive.arm.gov/), seven FLUXNET towers (Hyytiala, Tharandt, Loobos, Bondville, Walker Branch Watershed, Black Hills, and Mead Rain Fed,(downloaded from http://daac.ornl.gov/FLUXNET/fluxnet.html), and three flux towers in China (Miyun, Arou and Yingke) (Table 1). Except for the Chinese flux data, the data covers the period from 2000 to 2005, and each tower provides at least one year of reliable data. ET collected at the ARM flux towers of the Southern Great Plains of the US was measured by the Energy Balance Bowen Ratio (EBBR) method, while the ET collected at the other ten flux towers was measured by the Eddy Covariance (ECOR) method. Although the ECOR method is considered best for directly measuring heat fluxes in global measurement experiments (Baldocchi et al., 2001), we selected the method proposed by Twine et al. (2000) to correct the ET from the FLUXNET towers and Chinese flux towers, due to the problem of energy imbalance. The corrected method is as follows:

$$ET = \frac{ET_{EC}}{R_c} \tag{1}$$

$$R_c = \frac{ET_{EC} + H_{EC}}{R_n - G} \tag{2}$$

Here, ET is the corrected evapotranspiration. ET_{EC} and H_{EC} are the original evapotranspiration, and the sensible heat flux measured by the EC method, respectively. R_c is the energy closure ratio. R_n is the surface net radiation, and G is the ground heat flux.

We also used the monthly PDSI products derived from the NCAR CGD's Climate Analysis Section dataset (http://www.cgd.ucar.edu/cas/catalog/climind/pdsi.html) with a 2.5 degree spatial resolution, for the period from 1984 to 2002. To highlight the obvious features of both PDSI and EDI, we interpolated the PDSI products into 1 degree from a 2.5 degree spatial resolution. Moreover, we used the monthly latent heat flux at a 1 degree spatial resolution, obtained from the GSWP-2 multiple-

Table 1
The locations, latitude (Lat), longitude (Lon), land cover types, measurement method, project names, and time-periods for the 22 flux towers. ET (W/m^2) were measured using the Energy Balance Bowen Ratio (EBBR) method at all 12 ARM EF flux towers on the Southern Great Plains of the US, while the eddy covariance (ECOR) method was used to measure ET at the other 10 flux towers.

Site	Latitude, longitude	Land cover	Measurement method	Project	Time period
Hillsboro, Kansas: EF02, US	38.31°N, 97.30°W	Grass	EBBR	ARM	2003–2005
Plevna, Kansas: EF04, US	37.95°N, 98.33°W	Rangeland (ungrazed)	EBBR	ARM	2003–2005
Elk Falls, Kansas: EF07, US	37.38°N, 96.18°W	Pasture	EBBR	ARM	2003–2005
Coldwater, Kansas: EF08, US	37.33°N, 99.31°W	Rangeland	EBBR	ARM	2003–2005
Ashton, Kansas: EF09, US	37.13°N, 97.27°W	Pasture	EBBR	ARM	2003–2005
Pawhuska, Oklahoma: EF12, US	36.84°N, 96.43°W	Native prairie	EBBR	ARM	2003–2005
Lamont, Oklahoma: EF13, US	36.61°N, 97.49°W	Pasture and wheat	EBBR	ARM	2003–2005
Ringwood, Oklahoma: EF15, US	36.43°N, 98.28°W	Pasture	EBBR	ARM	2003–2005
Morris, Oklahoma: EF18, US	35.69°N, 95.86°W	Pasture	EBBR	ARM	2003–2005
El Reno, Oklahoma: EF19, US	35.56°N, 98.02°W	Pasture (ungrazed)	EBBR	ARM	2003–2005
Meeker, Oklahoma: EF20, US	35.56°N, 96.99°W	Pasture	EBBR	ARM	2003–2005
Cement, Oklahoma: EF26, US	34.96°N, 98.08°W	Pasture	EBBR	ARM	2003–2005
Hyytiala, Finland	61.85°N, 24.28°W	Scots pine	ECOR	FLUXNET	2000
Tharandt, Germany	50.97°N, 13.67°W	Norway Spruce	ECOR	FLUXNET	2000
Loobos, Netherlands	52.17°N, 44.63°W	Scots pine	ECOR	FLUXNET	2000
Bondville, Illinois, US	40.05°N, 88.37°W	Crop	ECOR	FLUXNET	2003–2005
Walker Branch Watershed, Tennessee, US	35.96°N, 84.29°W	Deciduous broadleaf forest	ECOR	FLUXNET	2003–2005
Black Hills, South Dakota, US	44.16°N, 103.65°W	Evergreen forest (Conifer)	ECOR	FLUXNET	2003–2005
Mead Rain Fed, Nebraska, US	41.16°N, 96.47°W	Rainfed maize	ECOR	FLUXNET	2003–2005
Miyun, Beijing, China	40.63°N, 117.32°E	Mixture	ECOR	–	2008 (July–September)
Arou, Qinghai, China	38.04°N, 100.46°E	Alpine grass	ECOR	–	2008 (July–September)
Yingke, Gansu, China	38.86°N, 100.41°E	Crop	ECOR	–	2008 (July–September)

model average datasets from January 1986 to December 1995 (http://haneda.tkl.iis.u-tokyo.ac.jp/gswp2/), and compared it with our estimated ET.

2.2. The hybrid ET model

In our algorithm, the landscape is simplified as a mixture of bare soil and vegetation elements. The proportion of vegetation is the fractional vegetation cover (f_{veg}), which can be estimated from the normalized difference vegetation index (NDVI) based upon satellite data. Assuming that the coupled energy transfer between bare soil and vegetation is negligible, the total ET in a pixel is equal to the combination of the ET from bare soil (ET_{soil}) and from vegetation (ET_{veg}) (Kustas and Norman, 1999; Nishida et al., 2003; Norman et al., 2003; Zhang et al., 2008; Leuning et al., 2008), namely:

$$ET = (1 - f_{veg})ET_{soil} + f_{veg}ET_{veg} \tag{3}$$

$$f_{veg} = \frac{NDVI - NDVI_{\min}}{NDVI_{\max} - NDVI_{\min}}, \tag{4}$$

where $NDVI_{\max}$ and $NDVI_{\min}$ are the NDVI of full vegetation ($f_{veg} = 1$) and bare soil ($f_{veg} = 0$), which are set as seasonally and geographically invariant constants of 0.95 and 0.05, respectively.

We also introduce the evaporation fraction (EF), which is defined as the ratio of ET to the available energy (Q) (W/m^2) (Shuttleworth et al., 1989; Nishida et al., 2003):

$$EF = \frac{ET}{Q} \tag{5}$$

Here Q is the difference between the net radiation (R_n) and the ground heat transfer (G). In our method, we set G as G_0R_n and G_0 is an empirical coefficient. Thus, we can express the EF as:

$$EF = \frac{ET}{Q} = \frac{ET}{R_n - G} = \frac{ET}{(1 - G_0)R_n} \tag{6}$$

At the same time, we can use the EF to describe both the ET_{soil} and ET_{veg}:

$$ET_{soil} = Q_{soil}EF_{soil} = a_0Q * EF_{soil} = a_0(1 - G_0)R_nEF_{soil} \tag{7}$$

$$ET_{veg} = Q_{veg}EF_{veg} = a_1Q * EF_{veg} = a_1(1 - G_0)R_nEF_{veg} \tag{8}$$

In Eqs. (7) and (8) above, Q_{soil} denotes the energy available from bare soil, Q_{veg} denotes the energy available from vegetation, EF_{soil} refers to the evaporation fraction of bare soil, and EF_{veg} refers to the evaporation fraction of vegetation. Here, we set Q_{soil} and Q_{veg} as a_0Q and a_1Q, respectively. a_0 and a_1 are empirical coefficients.

In this paper, to estimate the ET_{soil} and ET_{veg} successfully, EF_{soil} and EF_{veg}, which are the most important variables, must be calculated using the air temperature, net radiation, NDVI, and the diurnal air temperature range ($T_{\max} - T_{\min}$).

As for EF_{soil}, Nishida et al. (2003) revised the energy budget over bare soil based on the maximum surface temperature ($T_{soil,\max}$) and the actual surface temperature (T_{soil}) of bare soil, as well as the air temperature (T_a), and gave the following formula:

$$EF_{soil} = \frac{Q_{soil0}}{Q_{soil}}\frac{T_{soil,\max} - T_{soil}}{T_{soil,\max} - T_a} = \frac{Q_{soil0}}{Q_{soil}}\left(1 + \frac{T_a - T_{soil}}{T_{soil,\max} - T_a}\right), \tag{9}$$

where Q_{soil0} is the available energy (W/m^2) when T_{soil} is equal to T_a.

Eq. (9) indicates that EF_{soil} is closely related to the gradient of temperature, which may reflect soil moisture, though this gradient may not be used in regions having a known variability in surface moisture. Goward et al. (2002) and Zhang et al. (2003) also considered surface net radiation and soil moisture as the main factors that alter the surface ET of bare soil, an approach that is consistent with the report of Wang et al. (2006). Wang and Liang (2008) replaced soil moisture with the diurnal air temperature range ($T_{\max} - T_{\min}$), and considered the value of ET/R_n to be closely related to the daytime-averaged air temperature, NDVI, and the diurnal air temperature range, by taking advantage of satellite measurements and the ARM ground-measured data from the Southern Great Plains (SGP).

To reduce the complexity of the EF_{soil} algorithm in Eq. (9), we assume that Q_{soil0}/Q_{soil} and $T_a - T_{soil}$ are all invariant constants. To calculate EF_{soil} approximately using air temperature, we can replace $T_{soil,\max} - T_a$ with the diurnal air temperature range ($T_{\max} - T_{\min}$) to simplify the EF_{soil} by adding the empirical coefficients. These assumptions may generate some biases for bare soil evaporation estimation, but our results from independent validations, which are given in Section 3.1, support the reliability of our simplification. Thus, EF_{soil} can be expressed as:

$$EF_{soil} = b_0 + \frac{b_1}{T_{\max} - T_{\min}}, \tag{10}$$

where T_{max} is the daily maximum air temperature, T_{min} is the daily minimum air temperature, and b_0 and b_1 are all the empirical coefficients. In our method, we considered that daily satellite LST products are not available under cloudy conditions, and therefore selected air temperature as a replacement.

As for EF_{veg}, assuming that the entire available energy is dissipated as ET over dense vegetation, Nishida et al. (2003) provided the following formulation for the analysis of EF_{veg}:

$$EF_{veg} = \frac{\alpha\Delta}{\Delta + \gamma(1 + r_c/2r_a)} \tag{11}$$

$$\frac{1}{r_c} = \frac{f_1(T_a)f_2(VPD)f_3(PAR)f_4(\Psi)f_5(CO_2)}{r_{c_min}} + \frac{1}{r_{cuticle}} \tag{12}$$

Here, Δ is a derivative of the saturated vapor pressure in terms of temperature, γ is the psychrometric constant, the value of α is generally accepted as 1.26, r_a is the aerodynamic resistance, r_c is the surface resistance of the vegetation canopy, r_{c_min} is the minimum resistance, $r_{cuticle}$ is the canopy resistance related to diffusion through the cuticle layer of leaves, VPD is the vapor pressure deficit, PAR is the photosynthetic active radiation, and Ψ is the soil water potential.

Both Eqs. (11) and (12) show that vegetation transpiration is mainly controlled by aerodynamic resistance and canopy conductance (Kustas and Norman, 1999; Norman et al., 2003; Nishida et al., 2003; Mu et al., 2007; Zhang et al., 2008; Tang et al., 2010). Aerodynamic resistance is affected by wind speed. Canopy conductance is sensitive to the diurnal changes in absorbed photosynthetically active radiation (PAR), air temperature, Vapor Pressure Deficit (VPD), atmospheric CO_2 concentration and soil moisture near the roots (Jarvis, 1976; Mu et al., 2007). Some studies have shown that air temperature can be a surrogate for VPD (Tanaka et al., 2000).

Our method is to develop a linear combination of wind speed, PAR, air temperature, Vapor Pressure Deficit (VPD), atmospheric CO_2 concentration, and soil moisture near the roots to approximately simulate the results of Eq. (11). However, because wind speed, VPD, and CO_2 concentration are difficult to estimate from satellite data, we drop the terms of wind speed, VPD and CO_2 concentration. Additionally, we select R_n to replace PAR due to their approximately linear relationship. Similarly, the reciprocal of the diurnal air temperature range ($1/(T_{max} - T_{min})$) was selected to denote the soil moisture near the roots. Thus, we further combine these factors to obtain:

$$EF_{soil} = b_2 + b_3T_a + b_4R_n + \frac{b_5}{T_{max} - T_{min}}, \tag{13}$$

where b_i ($i = 2, \ldots, 5$) is the empirical coefficient. Such simplifications may inevitably introduce errors in certain cases, but on a scale that is acceptable for large-scale *ET* estimations.

By the combination of Eqs. (3), (4), (7), (8), (10) and (13), we obtain the entire ET:

$$ET = \left(1 - \frac{NDVI - 0.05}{0.95 - 0.05}\right) a_0(1 - G_0)R_n \left(b_0 + \frac{b_1}{T_{max} - T_{min}}\right) + \frac{NDVI - 0.05}{0.95 - 0.05} a_1(1 - G_0)R_n \left(b_2 + b_3T_a + b_4R_n + \frac{b_5}{T_{max} - T_{min}}\right) \tag{14}$$

We further simplify our model by integrating a series of empirical coefficients in order to propose a hybrid regression equation based on Eq. (14):

$$ET = R_n^2(c_1NDVI - c_2) + R_n\left(c_3 + c_4T_a + \frac{c_5}{T_{max} - T_{min}}\right) + R_n\left(c_6 + c_7T_a + \frac{c_8}{T_{max} - T_{min}}\right) NDVI \tag{15}$$

c_i ($i = 1, \ldots, 8$) is the empirical coefficient and it can be calibrated by linear regression using the observed data collected from a sufficient number of representative flux towers. Although Eq. (15) has been developed from a daily time-step, it can also be used to estimate monthly ET by taking advantage of monthly input parameters, because in this model, monthly forcing data can be calculated from the averaged daily input data. In Section 3.1, we independently validate the hybrid ET model for daily and monthly time-steps.

The hybrid model has two advantages. First, it is based on a linear two-source land surface ET model, which treats land surface as a composite of bare soil and vegetation with different Land Surface Temperatures (LST), albedo, and fluxes. Second, this model inherits the operability and applicability of a simple empirical model and can be applied to a range of vegetation and soil moisture stress conditions for large-scale ET estimations.

2.3. Estimation of potential evapotranspiration

Potential ET (PET) represents the ideal evaporation rate for capturing the response to forcing variables if soil moisture is unlimited. The accurate estimation of global PET is a significant challenge due to the complexity of the global land cover and vegetation types. To minimize the need for meteorological data but without decreasing the accuracy of the global PET estimates, we adopted the Hargreaves method to estimate PET. This method is much simpler for practical use because it requires only two easily accessible parameters: temperature and solar energy (Hargreaves et al., 1985; Hargreaves, 1989, 1994). Although the Hargreaves method performs effectively mainly for well-cropped grass, for exploration of the validity of the Evaporative Drought Index (EDI), the results from this method can be accepted on a global scale in this paper. Using the Hargreaves model, the PET can be easily estimated from NCEP-2 data. The Hargreaves model is expressed as follows:

$$PET = 0.0023R_a(T_{mean} + 17.8)\sqrt{T_{max} - T_{min}} \tag{16}$$

Here, PET is the potential evapotranspiration (mm/day) and R_a is the extraterrestrial solar incident radiation (MJ m^{-2} day^{-1}). The difference between R_a and R_s is that R_a is solar radiation at the top of atmosphere, which depends on the solar zenith angle; while R_s is the surface solar radiation, which depends on different parameters, including clouds, aerosols, and atmospheric water vapor content. Bibliographical resources (Mimikou and Baltas, 2002) provide R_a as a function of season and latitude in a tabular form.

2.4. EDI anomalies analysis and normalized calculation

To highlight the difference between drought indices for continuous years and comparability with the Palmer Drought Severity Index (PDSI), the EDI map depicts anomalies in the monthly and multi-year average values for a period of *n* years.

$$\Delta\bar{v}(m, y, i, j) = \bar{v}(m, y, i, j) - \frac{1}{n}\sum_{y=1}^{n}\bar{v}(m, y, i, j), \tag{17}$$

where $\bar{v}(m, y, i, j)$ is an output variable for month *m*, year is *y*, and pixel locations are *i*, *j*. Based on Eq. (17), the differences between EDI and PDSI from 1984 to 2002 are presented to execute long-term global surface drought mapping.

To illustrate the variation of EDI and PDSI during 1984–2002 across global continents (except for Antarctica), the average monthly $\bar{v}(m, y, i, j)$ for all pixels has been calculated using Eq. (18). The monthly normalized PDSI and EDI anomalies can then be determined based on Eqs. (19) and (20), respectively. Normalized EDI anomalies obtained using Eq. (20) are used to keep a consistent

variation for normalized PDSI anomalies, because both a higher EDI and a lower PDSI indicate dryer conditions.

$$\Delta\overline{AV}(m,y) = \frac{1}{S}\sum_{ij=1}^{S}\Delta\bar{v}(m,y,i,j) \tag{18}$$

$$N_v = \frac{\Delta\overline{AV}(m,y) - \Delta\overline{AV}(m,y)_{\min}}{\Delta\overline{AV}(m,y)_{\max} - \Delta\overline{AV}(m,y)_{\min}} \tag{19}$$

or

$$N_v = \frac{\Delta\overline{AV}(m,y)_{\max} - \Delta\overline{AV}(m,y)}{\Delta\overline{AV}(m,y)_{\max} - \Delta\overline{AV}(m,y)_{\min}}, \tag{20}$$

where $\Delta\overline{AV}(m,y)$ is the average monthly $\Delta\bar{v}(m,y,i,j)$ for all pixels; S is the whole number of all pixels; N_v is the normalized $\Delta\overline{AV}(m,y)$; $\Delta\overline{AV}(m,y)_{\min}$ is the minimum value of the $\Delta\overline{AV}(m,y)$; and $\Delta\overline{AV}(m,y)_{\max}$ is the maximum value of the $\Delta\overline{AV}(m,y)$.

3. Results and discussions

3.1. Model validation

To fairly assess the accuracy of the ET estimation, we randomly divided the 22 flux towers listed in Table 1 into two groups and performed a series of cross-validations. The first group included 12 flux towers (EF02, EF07, EF12, EF15, EF19, EF20, Hyytiala, Loobos, Walker Branch Watershed, Mead Rain Fed, Miyun and Arou) and the second group was composed of the other 10 flux towers (Tables 2 and 3). We performed calibration by linearly regressing the eight parameters in Eq. (15) using the collected ground-measured data from the first group and independently validated the daily (or monthly) ET from the second group of flux towers. We also calibrated by linearly regressing the eight parameters in Eq. (15) using the second group data and independently validated the daily (or monthly) ET from the first group of flux towers.

Table 2
A summary of the statistics (bias, the Root Mean Square Error, RMSE, and the square of the correlation coefficients, R^2) of the comparison between ground-measured and estimated daily ET from the second group of flux towers, using the first group data to calibrate the eight parameters in Eq. (15). The bias and RMSE are in units of W/m^2.

Site	Bias	RMSE	R^2
Plevna, Kansas: EF04, US	12.95	22.75	0.80
Coldwater, Kansas: EF08, US	−0.84	20.86	0.71
Ashton, Kansas: EF09, US	−5.93	20.31	0.84
Lamont, Oklahoma: EF13, US	−1.52	22.17	0.72
Morris, Oklahoma: EF18, US	−6.72	15.57	0.91
Cement, Oklahoma: EF26, US	1.70	21.88	0.74
Tharandt, Germany	−0.98	21.80	0.62
Bondville, Illinois, US	0.62	17.77	0.77
Black Hills, South Dakota, US	8.07	18.92	0.63
Yingke, Gansu, China	−4.19	17.37	0.75
Average	0.74	20.40	0.76

Table 3
A summary of the statistics (bias, the Root Mean Square Error, RMSE, and the square of the correlation coefficients, R^2) used in the comparison between ground-measured and estimated daily ET for the first group of flux towers using the second group data to calibrate the eight parameters in Eq. (15). The bias and RMSE are in units of W/m^2.

Site	Bias	RMSE	R^2
Hillsboro, Kansas: EF02, US	−5.58	19.57	0.82
Elk Falls, Kansas: EF07, US	−12.91	25.97	0.75
Pawhuska, Oklahoma: EF12, US	−0.81	17.66	0.86
Ringwood, Oklahoma: EF15, US	−5.44	19.37	0.87
El Reno, Oklahoma: EF19, US	1.47	16.43	0.84
Meeker, Oklahoma: EF20, US	−0.93	18.83	0.80
Hyytiala, Finland	10.26	16.66	0.80
Loobos, Netherlands	−2.45	13.06	0.81
Walker Branch Watershed, Tennessee, US	3.67	15.12	0.90
Mead Rain Fed, Nebraska, US	9.35	17.41	0.85
Miyun, Beijing, China	5.43	18.42	0.76
Arou, Qinghai, China	−8.88	20.11	0.85
Average	−1.73	19.26	0.81

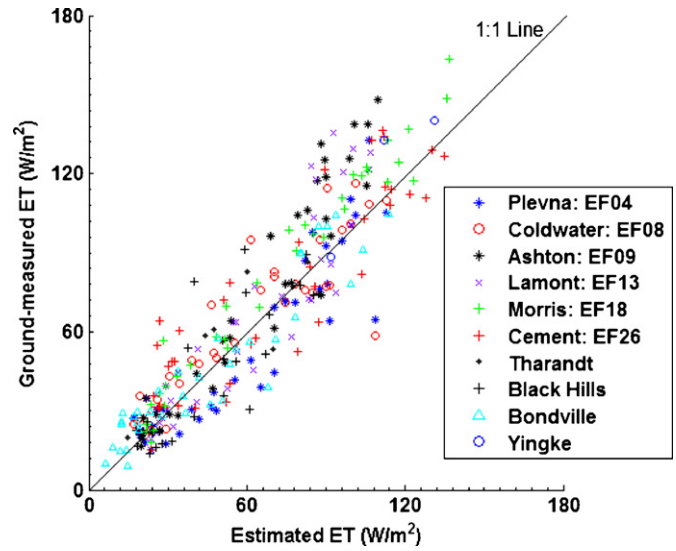

Fig. 1. Scatter plots of the predicted monthly ET and ground-measured ET for the second group of flux towers using the first group data to calibrate the eight parameters in Eq. (15).

Table 2 demonstrates the bias, the Root Mean Square Error (RMSE), and the square of correlation coefficients (R^2) of the comparison between the ground-measured and estimated daily ET from the second group of flux towers, using the first group data to calibrate the eight parameters in Eq. (15). We see that the bias of the estimated daily ET varies from −6.72 W/m^2 to 12.95 W/m^2, the R^2 varies from 0.62 to 0.91, and the RMSE varies from 15.57 W/m^2 to 22.75 W/m^2. Fig. 1 shows the good correspondence between the estimated monthly ET based on our hybrid model and the measured ET from the second group of flux towers. The R^2 for the entire second group flux towers is 0.84, though it varies from site to site, and the RMSE is 15.35 W/m^2 and the bias is −1.73 W/m^2. Similarly, Table 3 demonstrates that Eq. (15) accurately estimates the ET for the first group of flux towers using the second group data to calibrate the eight parameters in Eq. (15). One can see that the R^2 is greater than 0.75, the bias of the estimated daily ET deviating from the corresponding ground-measured ET varies from −12.91 W/m^2 to 10.26 W/m^2, and the RMSE varies from 13.06 W/m^2 to 25.97 W/m^2. Fig. 2 illustrates the good agreement between the estimated monthly ET based on our model versus the measured ET from the first group of flux towers. The overall correlation coefficient of a comparison between the measured and predicted monthly ET using Eq. (15) is 0.83, the RMSE is 12.88 W/m^2, and the bias is −3.59 W/m^2. Jiang and Islam (2001) documented an RMSE of 85.30 W/m^2 using the linear NDVI-LST spatial variation method from NOAA-AVHRR data and an interpolated surface net radiation map over the SGP area for 2001. Seguin et al. (1999) suggested that the required ET retrieval accuracy varies according to the application, but is typically 50 W/m^2. The accuracy of our study results meets this requirement.

The use of our ET algorithm, however, also produces biases between the ET estimates and the ET observations, which may reflect the influence of two factors. (1) There may be errors in the input data. The collected flux and meteorological data is typically at half-hour intervals. Using so few observation samples to calculate the daily input parameters can lead to errors (Desai et al., 2005). The uncertainty of MODIS NDVI products also limits our ability to

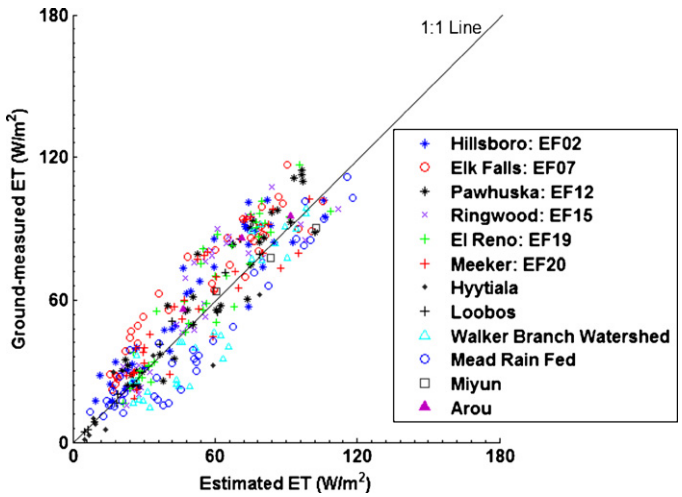

Fig. 2. Scatter plots of the predicted monthly ET and ground-measured ET for the first group of flux towers using the second group data to calibrate the eight parameters in Eq. (15).

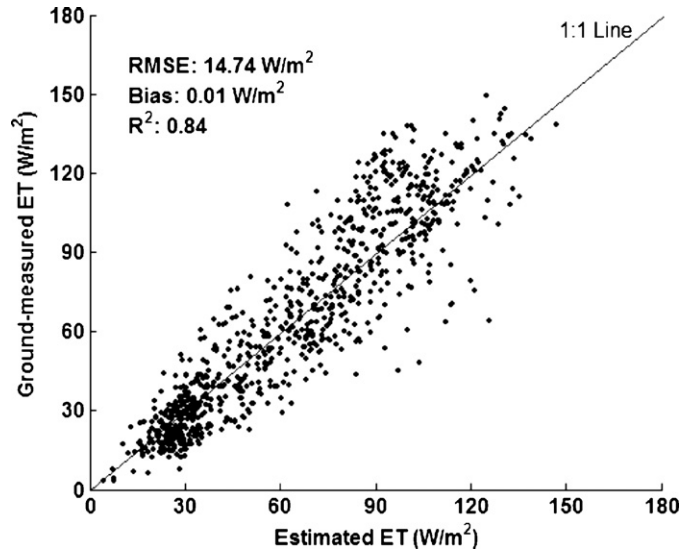

Fig. 3. Comparison of the 16-day daily estimated and ground-measured ET collected at all 22 sites shown in Table 1. The 16-day average was used because MODIS NDVI products have a 16-day interval.

obtain reliable estimates of the daily ET. (2) There are limitations in the algorithm. Though our ET model can work well for a wide range of land cover types, our algorithm may overestimate the ET for arid regions where the ET is relatively small, such as over the great deserts of North Africa. Further study is therefore needed to improve the ET algorithm for certain ecosystems, such as those in arid regions.

3.2. Global implementation of the ET estimation

We implemented the revised ET algorithm globally to further demonstrate its reliability. We selected R_n, NDVI, T_a, T_{max}, and T_{min}, as the input parameters to linearly regress to yield Eq. (21) for global ET estimation based on daily meteorological data, and MODIS NDVI composite products with a 1-km spatial resolution temporally interpolated from the 16-day averages covering 2000–2008 from all twenty-two flux towers (Table 1). Considering the variety of land cover that includes grass, rangeland, pastures, crop fields, forests, and mixed cover—including vegetation and bare soil—and considering that their locations also differ greatly from each other, we find these sufficiently representative for the purpose of estimating global ET (except for desert and glacier regions).

$$ET = R_n^2(0.00084NDVI - 0.000978) + R_n\left(0.3044 + 0.0029T_a + \frac{0.284}{T_{\max} - T_{\min}}\right) + R_n\left(0.1273 + 0.01T_a + \frac{0.065}{T_{\max} - T_{\min}}\right)NDVI \quad (21)$$

Fig. 3 shows scatter plots of a comparison between 16-day daily estimated and ground-measured ET using ground observation data. The 16-day average has been used here because the MODIS NDVI products are available for a 16-day interval. We observe that the bias of the estimated ET at all twenty-two sites is 0.01 W/m^2. The RMSE is 14.74 W/m^2 and the R^2 is about 0.84. The accuracy of the ET simulation can be used for estimating the global land surface ET.

Rigorous validation of global ET derived from the remote sensing radiation flux described here is difficult because it requires time-continuous flux measurements on a scale of at least 1 degree. Until now, such time-continuous flux measurements have not existed on a global scale. Moreover, the latent heat flux derived from reanalysis datasets, data assimilation, and global land model simulations also contains large uncertainties. To illustrate the validity of our hybrid ET model, we compared the monthly ET at a spatial resolution of $1^\circ \times 1^\circ$ as predicted by Eq. (21) to the 15-model-simulation-averaged ET from the Global Soil Wetness Project-2 (GSWP-2) (Dirmey et al., 2006; Wang and Liang, 2008), even though their results may indicate significant differences. The forcing data of our model includes global monthly GEWEX surface net radiation products, monthly AVHRR-GIMMS-NDVI datasets, monthly NCEP-2 reanalysis air mean temperature, and maximum and the minimum air temperature data from 1984 to 2002. GSWP-2 is an offline land surface model and its ET products are superior to the results of other individual models. It can therefore be considered as a reference dataset to evaluate our hybrid model.

One example of the evaluation of the hybrid ET model is a comparison of the estimated monthly ET of October 1986 using GEWEX, AVHRR-GIMMS-NDVI and NCEP-2 datasets with the latent heat flux from GSWP-2 in Fig. 4. Fig. 4(a) and (b) show similar spatial distribution patterns in both maps, though the ET over the central and southern areas of the US exhibit great differences. This discrepancy may be an error that was partially caused by the inaccuracy of the GEWEX and NCEP-2 data. We can see that the bias of the estimated ET that deviates from the GSWP-2 ET is 0.01 W/m^2 in Fig. 4(c). Furthermore, the RMSE is 16.24 W/m^2 and the R^2 is 0.76. This small positive bias may be partially attributed to our overestimate of ET over the desert and glacier regions.

Fig. 5 shows histograms of the R^2, bias, and RMSE of the comparison between the ET estimated by Eq. (21) and the corresponding GSWP-2 ET during the 120 months from January 1986 to December 1995. Fig. 5(a) shows a bias range of −4.54–10.19 W/m^2, with a mean bias of 6.15 W/m^2; Fig. 5(b) shows an R^2 range of 0.54–0.82, with a mean R^2 of 0.71; and Fig. 5(c) shows an RMSE range of 16.34–24.31 W/m^2, with a mean RMSE of 20.34 W/m^2. This bias may partly reflect the simulation bias of the hybrid ET model itself. The good agreement between the two independent datasets indicates that the hybrid ET model provides reliable information for global applications.

Global monthly ET products (except for Antarctica) from 1984 to 2002 have been obtained based on Eq. (21), though the ET over desert, snow and ice are overestimated. The month-to-month patterns for April through September of 2001 and 2002 reveal similar spatial distribution and seasonal shifts (Fig. 6). This seasonal interval was selected to cover most of the crop growing cycle—excluding snow cover. The major regions of northern Africa and Australia

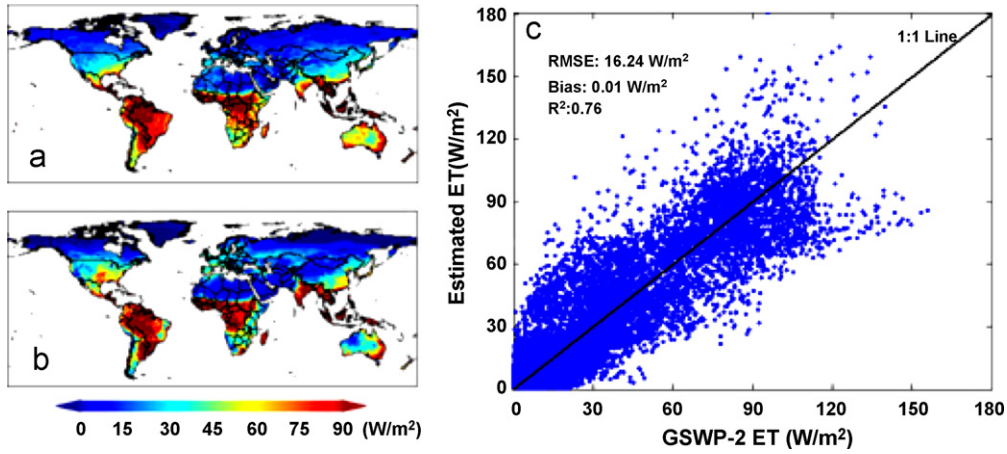

Fig. 4. An example of the comparison of monthly ET using GEWEX, AVHRR-GIMMS-NDVI and NCEP-2 datasets of October 1986, and the corresponding latent heat flux from the GSWP-2 datasets. (a) The spatial distribution of the estimated monthly ET obtained using Eq. (21) for October 1986; (b) spatial distribution of the corresponding GSWP-2 ET; and (c) scatter plots of the estimated monthly ET for October 1986 and the corresponding GSWP-2 ET.

remain consistently low throughout 2001 and 2002, while the southern hemispheric tropics remain consistently high. In the high northern latitudes, the global ET presents high variations with increases into the northern summer, which trail off in the autumn due to the major global change on a monthly scale. Though it is a challenge to give a detailed explanation for this variation in global ET, it may be attributed to the differences in temperature, precipitation, and vegetation growth conditions in different regions.

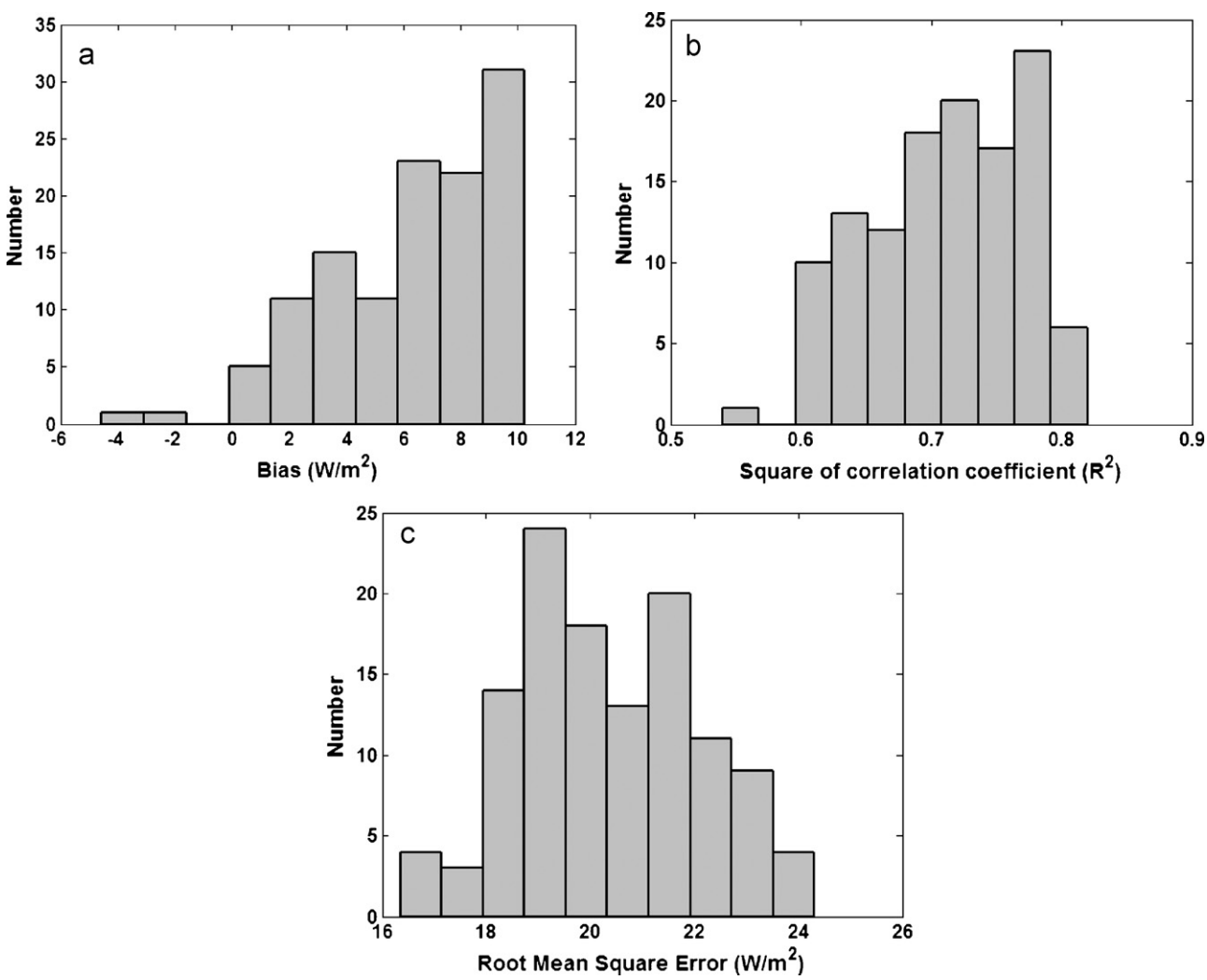

Fig. 5. Histograms of the (a) bias, (b) square of correlation coefficient (R^2), and (c) Root Mean Square Error (RMSE) used in the comparison between ET estimated using Eq. (21) and the corresponding GSWP-2 ET during the 120 months from January 1986 to December 1995.

Please cite this article in press as: Yao, Y., et al., Monitoring global land surface drought based on a hybrid evapotranspiration model. Int. J. Appl. Earth Observ. Geoinf. (2010), doi:10.1016/j.jag.2010.09.009

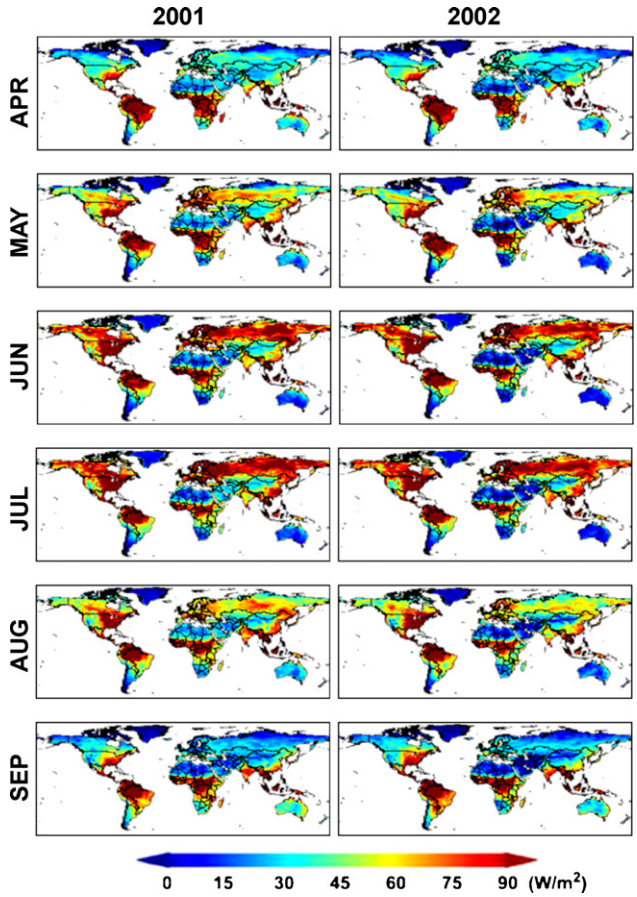

Fig. 6. Estimated global monthly ET for April–September of 2001–2002.

3.3. Global EDI anomalies in comparison with the Palmer Drought Severity Index

Palmer drought indices can reflect drought impacts over different time periods and incorporate antecedent precipitation, moisture supply and demand (Palmer, 1965). The Palmer moisture anomaly index (Z index), the Palmer Drought Severity Index (PDSI), and the Palmer Hydrologic Drought Severity Index (PHDSI) were developed for the monitoring of long-term surface drought conditions. Of these tools, PDSI has been most widely used to simulate the monthly moisture content of soil and to compare monthly anomalies of regions with variable climates and seasons (Palmer, 1965; Dai et al., 2004; Szep et al., 2005). Considering that it is one of the most common indices used worldwide, PDSI is most comparable to the EDI, even as its functional deficiencies are well known.

To highlight the extremely dry conditions during 1984–2002, the monthly EDI deviations ($\Delta\overline{EDI}$) and PDSI deviations ($\Delta\overline{PDSI}$) average were calculated, because EDI anomalies ($\Delta\overline{EDI}$) or PDSI deviations ($\Delta\overline{PDSI}$) can emphasize the differences in EDI or PDSI variation by removing their identical features over a long period of time. To improve the comparability of the EDI anomalies ($\Delta\overline{EDI}$) and PDSI deviations ($\Delta\overline{PDSI}$), monthly normalized EDI anomalies ($\Delta\overline{EDI}$) and PDSI deviations ($\Delta\overline{PDSI}$) averaged for all pixels (except for Antarctica) were calculated. Fig. 7 shows the temporal variation of monthly normalized EDI and PDSI anomalies from January 1984 to December 2002. One can see that the monthly curves are in good agreement from January 1990 to December 2002, and the statistical analysis results show that the correlation coefficient between them is greater than 0.7. However, there is an obvious bias of the normalized EDI anomalies ($\Delta\overline{EDI}$) and

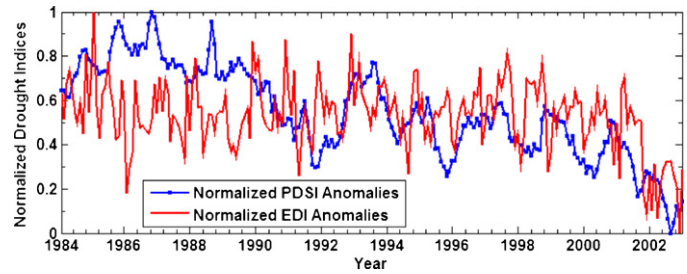

Fig. 7. Temporal variation of monthly normalized EDI and PDSI anomalies from January 1984 to December 2002.

PDSI deviations ($\Delta\overline{PDSI}$) from January 1984 to December 1989, and EDI shows a larger variation than PDSI (Fig. 7), particularly for January 1986. This discrepancy is obvious because PDSI is estimated using antecedent precipitation while EDI is primarily driven by radiation, the vegetation index, and the temperature dataset. In general, satellite-based EDI may serve as an after-effect drought indicator, since there are time lags between occurrences of drought in some consecutive time periods, and the ET changes because healthy vegetation can maintain a high ET for longer intervals after rain events due to sufficient soil moisture from vegetation roots, a dynamic which coincides with the results of Anderson et al. (2007a,b). Moreover, the errors of an input dataset that includes GEWEX radiation products, AVHRR-GIMMS NDVI products, and NCEP-2 data, along with the biases of the ET and PET models, may be the primary source of the biases of satellite-based EDI products.

To analyze the spatial pattern in both $\Delta\overline{EDI}$ and $\Delta\overline{PDSI}$ from 1984 to 2002, we mapped the monthly EDI deviations ($\Delta\overline{EDI}$) and PDSI deviations ($\Delta\overline{PDSI}$) for April through September of 2001–2002 (Fig. 8), because of the relatively wet conditions of 2001 and the dry conditions of 2002 shown in Fig. 7.

In 2001, both indices show that the western regions of North America, the central regions of Africa, the east of South America, east Asia (mainly eastern China), and southeast Australia were dryer during April, as can be seen in both $\Delta\overline{EDI}$ and $\Delta\overline{PDSI}$, a result which is consistent with those of previous studies (White et al., 2003; Dai et al., 2004; Bordi et al., 2006; Kim et al., 2009; Zhao and Running, 2010). By May, the regions of the western areas of South America and Europe, north Asia, southern Africa, and the central and eastern areas of North America become wetter due to the heavy monthly precipitation, and the dry conditions shift to the eastern coastal regions of each continent. In June, both indices show extremely dry conditions prevalent from west Asia to Southeast Asia, while the eastern areas of North America become wetter. In July, dry conditions still exist in Southeast Asia in the $\Delta\overline{EDI}$ map, while this region appears wet in the $\Delta\overline{PDSI}$ map. These differences may well reflect the slight decreases of the southeast Asia ET due to the decline in net radiation caused by industrial activity and the vegetation coverage fraction caused by human activity (Zhou et al., 2004). From August to September, extreme drought conditions affect much of the southeast area of Australia, though there is a slight difference in both $\Delta\overline{EDI}$ and $\Delta\overline{PDSI}$ maps from April to September. For example, the $\Delta\overline{PDSI}$ map indicates that during this period, there was an almost continuous band of extreme drought stretching across North Africa, but the $\Delta\overline{EDI}$ map indicates an opposite trend. These discrepancies between the EDI and PDSI maps may indicate that our hybrid ET model may generate overestimations over the great deserts of North Africa, where the ET is relatively small.

In contrast to 2001, both indices for 2002 show the entire Australian continent became dryer from April to September. The $\Delta\overline{EDI}$ map indicates the obvious dryer condition that prevails in the

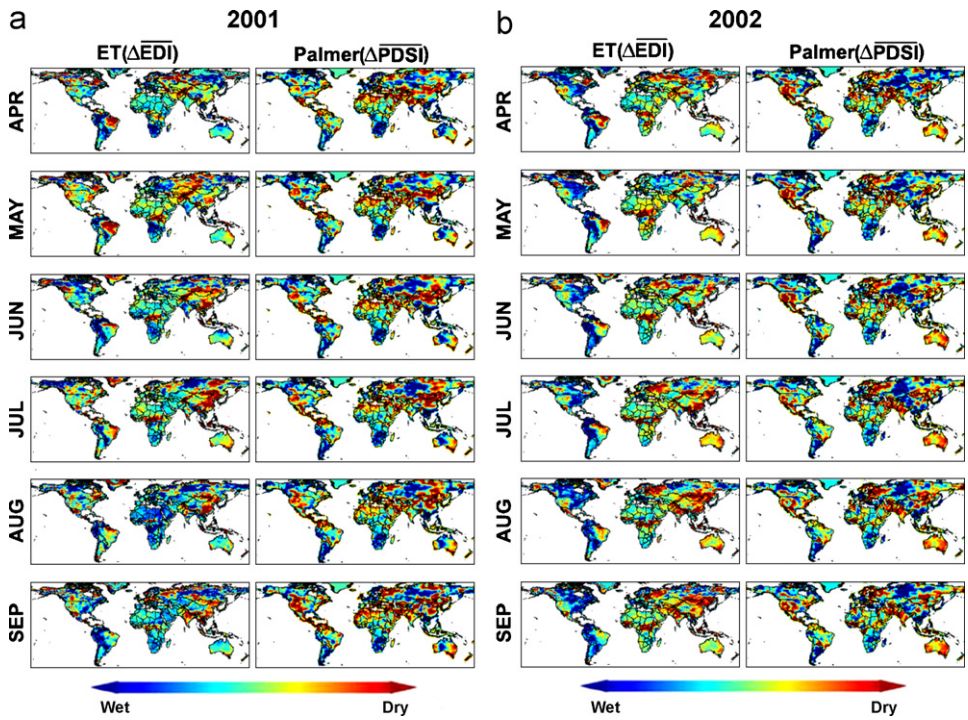

Fig. 8. (a) Monthly anomalies of EDI ($\Delta\overline{EDI}$) compared with anomalies in the PDSI ($\Delta\overline{PDSI}$) for April–September of 2001–2002. (b) Monthly anomalies of EDI ($\Delta\overline{EDI}$) compared with anomalies in the PDSI ($\Delta\overline{PDSI}$) for April–September of 2001–2002.

southern areas of Africa in both April and May, but the $\Delta\overline{PDSI}$ map did not capture this detail. This difference may be partially explained by both the energy radiation driving the change in EDI and the precipitation controlling the change in PDSI. The wet conditions in Europe became dryer in June, and overall, the trends in the $\Delta\overline{EDI}$ map are consistent with those in the $\Delta\overline{PDSI}$ map. By July, both $\Delta\overline{EDI}$ and $\Delta\overline{PDSI}$ highlight the dry conditions that prevailed in east Asia and the western areas of North America because these regions suffered from lack of rain. This finding is consistent with the reported Drought Monitor records of the US These extreme dry conditions persisted into the month of August. However, both the eastern areas of North America and the western areas of South America are wetter in the $\Delta\overline{EDI}$ map than in the $\Delta\overline{PDSI}$ map. This wet condition was aggravated to some extent in September. It is a challenge to speculate in detail as to the possible causes of the EDI changes over all continental regions (except for Antarctica), because the factors of net radiation, air temperature, precipitation, vapor pressure deficit, and land cover all contribute to the EDI for land surface drought monitoring.

In general, there is a good correspondence between the spatio-temporal pattern in both $\Delta\overline{EDI}$ and $\Delta\overline{PDSI}$ maps. They both use independent methods for surface dryness detection, because the input parameters for EDI include surface net radiation, air temperature, NDVI, and diurnal air temperature ranges, while the PDSI requires antecedent precipitation data. The good agreement of the spatio-temporal patterns in both the $\Delta\overline{EDI}$ and $\Delta\overline{PDSI}$ maps indicates that the EDI based on net radiation, air temperature, NDVI, and diurnal air temperature ranges can provide a valuable method for monitoring global drought events using satellite and NCEP-2 data.

4. Conclusions

The hybrid ET model described in this paper, which is based on the surface energy balance and empirical equations, has a demonstrated utility in mapping and estimating ET on a global scale. The hybrid ET model is a significantly simplified, two-source evaporation empirical model in which the landscape is considered as a mixture of bare soil and vegetation. Moreover, the model has the operability and flexibility to incorporate satellite products to improve its accuracy. Based on this ET model, the Evaporative Drought Index (EDI) was adopted to highlight surface dryness by integrating information regarding energy fluxes in response to soil moisture stress, and the model then proved its effectiveness in global drought monitoring.

Global monthly EDI from 1984 to 2002 were produced using the hybrid ET model with the net radiation, vegetation index, temperature, and the diurnal difference in temperatures from GEWEX, AVHRR-GIMMS-NDVI, and NCEP Reanalysis-2 data. To assess the accuracy of the hybrid ET model, we randomly divided the 22 flux towers into two groups and performed a series of cross-validations using ground measurements collected from the corresponding flux towers. The validation results from the second group of flux towers using the first group data to calibrate them, show that the daily bias varies from $-6.72\,W/m^2$ to $12.95\,W/m^2$ and the average monthly bias is $-1.73\,W/m^2$. Similarly the validation results for the first group flux towers using the second group data to calibrate them, show that the daily bias varies from $-12.91\,W/m^2$ to $10.26\,W/m^2$ and the average monthly bias is $-3.59\,W/m^2$. To evaluate the reliability of the hybrid ET model on a global scale, we compared the estimated ET from GEWEX, AVHRR-GIMMS-NDVI and NECP-2 data with the latent heat flux from GSWP-2 datasets, and found that both were in good agreement. This further indicates that the hybrid ET model can provide reliable information for global applications. We compared the EDI with the Palmer Drought Severity Index (PDSI), and the results show a good correspondence between their spatial-temporal patterns. Since an EDI based on the hybrid ET model can accurately interpret variations in soil moisture caused by drought stress, it can also provide a favorable range of sensitivity resolution to detect surface drought events. Further exploration of the EDI based on the hybrid ET model, and the advantages it offers for different eco-systems, will continue to be the focus of our future research efforts.

Please cite this article in press as: Yao, Y., et al., Monitoring global land surface drought based on a hybrid evapotranspiration model. Int. J. Appl. Earth Observ. Geoinf. (2010), doi:10.1016/j.jag.2010.09.009

Acknowledgments

The authors would like to thank Professor Shaomin Liu of Beijing Normal University, China for providing flux observation data from three Chinese flux towers (Miyun, Arou and Yingke). The authors also thank the anonymous reviewers for their critical and helpful comments and suggestions. The authors would also like to extend their thanks to Professor Renhua Zhang of the Institute of Geographic Sciences and Natural Resources Research, CAS, and to Dr. Xiaotong Zhang and Dr. Xiufang Zhu of University of Maryland, USA for their help. This work was partially supported by NASA (No. NNX08AC53G), the R&D Special Fund for Public Welfare Industry of China (Meteorology) (No. GYHY 200806022), the High-Tech Research and Development Program of China (No. 2008AA121806-04 and No. 2009AA12Z128), the China Postdoctoral Science Foundation Funded Project (No. 20090450223), and the Chinese Fellowship Program (No. 2008601058).

References

Abramopoulos, F., Rosenzweig, C., Choudhury, B., 1988. Improved ground hydrology calculations for global climate models (GCMs): soil water movement and evapotranspiration. J. Appl. Meteorol. Climatol. 1, 921–941.
Allen, R.G., Tasumi, M., Trezza, R., 2007a. Satellite-based energy balance for mapping evapotranspiration with internalized calibration (METRIC): model. J. Irrig. Drain. Eng. ASCE 133 (4), 380–394.
Allen, R.G., Tasumi, M., Trezza, R., 2007b. Satellite-based energy balance for mapping evapotranspiration with internalized calibration (METRIC): applications. J. Irrig. Drain. Eng. ASCE 133 (4), 395–406.
Anderson, M.C., Norman, J.M., Mecikalski, J.R., Otkin, J.A., Kustas, W.P., 2007a. A climatological study of evapotranspiration and moisture stress across the continental United States based on thermal remote sensing: 1. Model formulation. J. Geophys. Res. 112, D10117.
Anderson, M.C., Norman, J.M., Mecikalski, J.R., Otkin, J.A., Kustas, W.P., 2007b. A climatological study of evapotranspiration and moisture stress across the continental United States based on thermal remote sensing: 2. Surface moisture climatology. J. Geophys. Res. 112, D11112.
Arnold, J.G., Srinivasan, R., Muttiah, R.S., Williams, J.R., 1998a. Large area hydrologic modeling and assessment. Part I: model development. J. Am. Water Resour. Assoc. 34 (1), 73–89.
Arnold, J.G., Srinivasan, R., Muttiah, R.S., Williams, J.R., 1998b. Large area hydrologic modeling and assessment. Part II: model application. J. Am. Water Resour. Assoc. 34 (1), 91–101.
Baldocchi, D., Falge, E., Gu, L.H., et al., 2001. FLUXNET: a new tool to study the temporal and spatial variability of ecosystem-scale carbon dioxide, water vapor and energy flux densities. Bull. Am. Meteorol. Soc. 82 (11), 2415–2434.
Bastiaanssen, W.G.M., Menenti, M., Feddes, R.A., Holtslag, A.A.M., 1998a. A remote sensing surface energy balance algorithm for land. I. Formulation. J. Hydrometeorol. 213 (1–4), 198–212.
Bastiaanssen, W.G.M., Menenti, M., Feddes, R.A., Holtslag, A.A.M., 1998b. A remote sensing surface energy balance algorithm for land. II. Validation. J. Hydrometeorol. 213 (1–4), 213–229.
Bordi, I., Fraedrich, K., Petitta, M., Sutera, A., 2006. Large-scale assessment of drought variability based on NCEP/NCAR and ERA-40 re-analyses. Water Resour. Manage. 20 (6), 899–915.
Choudhury, B.J., 1983. Simulating the effects of weather variables and soil water potential on a corn crop canopy temperature. Agric. Meteorol. 29, 169–182.
Cleugh, H.A., Leuning, R., Mu, Q., Running, S.W., 2007. Regional evaporation estimates from flux tower and MODIS satellite data. Remote Sens. Environ. 106 (3), 285–304.
Dai, A.G., Trenberth, K.E., Qian, T., 2004. A global data set of Palmer Drought Severity Index for 1870–2002: relationship with soil moisture and effects of surface warming. J. Hydrometeorol. 5 (6), 1117–1130.
Desai, A.R., Bolstad, P.V., Cook, B.D., Davis, K.J., Carey, E.V., 2005. Comparing net ecosystem exchange of carbon dioxide between an old-growth and mature forest in the upper Midwest, USA. Agric. For. Meteorol. 128 (1–2), 33–55.
Dirmey, P.A., Gao, X.A., Zhao, M., et al., 2006. GSWP-2: multimodel analysis and implications for our perception of the land surface. B. Am. Meteorol. Soc. 87 (10), 1381–1397.
Fisher, J.B., Tu, K.P., Baldocchi, D.D., 2008. Global estimates of the land-atmosphere water flux based on monthly AVHRR and ISLSCP-II data, validated at 16 FLUXNET sites. Remote Sens. Environ. 112 (3), 901–919.
Ghulam, A., Li, Z.L., Qin, Q.M., Tong, Q.X., 2007. Exploration of the spectral space based on vegetation index and albedo for surface drought estimation. J. Appl. Remote Sens. 1, 013529.
Gillies, R.T., Carlson, T.N., Cui, J., Kustas, W.P., Humes, K.S., 1997. A verification of the 'triangle' method for obtaining surface soil water content and energy fluxes from remote measurements of the Normalized Difference Vegetation Index (NDVI) and surface radiant temperatures. Int. J. Remote Sens. 18 (15), 3145–3166.
Goward, S.N., Xue, Y.K., Czajkowski, K.P., 2002. Evaluating land surface moisture conditions from the remotely sensed temperature/vegetation index measurements: an exploration with the simplified simple biosphere model. Remote Sens. Environ. 79 (2–3), 225–242.
Hargreaves, G.H., 1989. Accuracy of estimated reference crop evapotranspiration. J. Irrig. Drain. Eng. ASCE 115 (6), 1000–1007.
Hargreaves, G.H., 1994. Defining and using reference evapotranspiration. J. Irrig. Drain. Eng. ASCE 120 (6), 1132–1139.
Hargreaves, G.L., Hargreaves, G.H., Riley, J.P., 1985. Irrigation water requirements for Senegal river basin. J. Irrig. Drain. Eng. ASCE 111 (3), 265–275.
Idso, S.B., Jackson, R.D., Printer, P.J., 1981. Measuring yield reducing plant water potential depressions in wheat by infrared thermometry. Irrig. Sci. 2 (4), 205–212.
Jackson, R.D., 1982. Soil moisture inferences from thermal infra-red measurements of vegetation temperatures. IEEE Trans. Geosci. Remote Sensing 20 (3), 282–286.
Jarvis, P.G., 1976. The interpretation of the variations in leaf water potential and stomatal conductance found in canopies in the field. Philos. Trans. R. Soc. Lond. Ser. B 273 (927), 593–610.
Jiang, L., Islam, S., 2001. Estimation of surface evaporation map over southern Great Plains using remote sensing data. Water Resour. Res. 37 (2), 329–340.
Kalma, J.D., Mcvicar, T.R., Mccabe, M.F., 2008. Estimating land surface evaporation: a review of methods using remotely sensed surface temperature data. Surv. Geophys. 29 (4–5), 421–469.
Kim, D.-W., Byun, H.-R., 2009. Future pattern of Asian drought under global warming scenario. Theor. Appl. Climatol. 98 (1–2), 137–150.
Kustas, W.P., Norman, J.M., 1999. Evaluation of soil and vegetation heat flux predictions using a simple two-source model with radiometric temperatures for partial canopy cover. Agric. For. Meteorol. 94 (1), 13–25.
Lambin, E.F., Ehrlich, D., 1996. The surface temperature-vegetative index space for land cover and land cover change analysis. Int. J. Remote Sens. 17 (3), 463–487.
Leuning, R., Zhang, Y.Q., Rajaud, A., Cleugh, H., Tu, K., 2008. A simple surface conductance model to estimate regional evaporation using MODIS leaf area index and the Penman-Monteith equation. Water Resour. Res. 44 (10), W10419.
Mahfouf, J.F., Noilhan, J., 1991. Comparative study of various formulations of evaporation from bare soil using in situ data. J. Appl. Meteorol. Climatol. 30 (9), 1354–1365.
McVicar, T.R., Jupp, D.L.B., 1998. The current and potential operational uses of remote sensing to aid decisions on drought exceptional circumstances in Australia: a review. Agric. Syst. 57 (3), 399–468.
Mimikou, M., Baltas, E., 2002. Technical hydrology, second edition. NTUA, 230 pp.
Moran, M.S., Clarke, T.R., Inoue, Y., Vidal, A., 1994. Estimating crop water deficit using the relation between surface–air temperature and spectral vegetation index. Remote Sens. Environ. 49 (3), 246–263.
Mu, Q.Z., Heinsch, F.A., Zhao, M.S., Running, S.W., 2007. Development of a global evapotranspiration algorithm based on MODIS and global meteorology data. Remote Sens. Environ. 111, 519–536.
Nishida, K., Nemani, R.R., Running, S.W., Glassy, J.M., 2003. An operational remote sensing algorithm of land surface evaporation. J. Geophys. Res. 108 (D9), 4270.
Norman, J.M., Anderson, M.C., Kustas, W.P., French, A.N., Mecikalski, J.R., Torn, R.D., Diak, G.R., Schmugge, T.J., Tanner, B.C.W., 2003. Remote sensing of surface energy fluxes at 10^1-m pixel resolutions. Water Resour. Res. 39 (8), 1221.
Palmer, W.C., 1965. Meteorological Drought, U.S. Weather Bur. Res., vol. 45. NOAA, Silver Spring, MD, 58 pp.
Priestley, C.H.B., Taylor, R.J., 1972. On the assessment of surface heat flux and evaporation using large-scale parameters. Month. Weather Rev. 100 (2), 81–92.
Robeson, S.M., 2008. Applied climatology: drought. Prog. Phys. Geogr. 32 (3), 303–309.
Seguin, B., Becker, F., Phulpin, T., et al., 1999. IRSUTE: a mini-satellite project for land surface heat flux estimation from field to regional scale. Remote Sens. Environ. 68 (3), 357–369.
Senay, G.B., Budde, M., Verdin, J.P., Melesse, A.M., 2007. A coupled remote sensing and simplified surface energy balance approach to estimate actual evapotranspiration from irrigated fields. Sensors 7 (6), 979–1000.
Shuttleworth, W.J., Gurney, R.J., Hsu, A.Y., Ormsby, J.P., 1989. FIFE: the variation in energy partition at surface flux sites. IAHS Publ. 186, 67–74.
Shuttleworth, W.J., Wallace, J.S., 1985. Evaporation from sparse crops—an energy combination theory. Q. J. R. Meteor. Soc. 111 (469), 839–855.
Song, J., Wesely, M.L., Coulter, R.L., Brandes, E.A., 2000. Estimating watershed evapotranspiration with PASS. Part I. Inferring root-zone moisture conditions using satellite data. J. Hydrometeorol. 1 (5), 447–461.
Szep, I.J., Mika, J., Dunkel, Z., 2005. Palmer drought severity index as soil moisture indicator: physical interpretation, statistical behavior and relation to global climate. Phys. Chem. Earth 30 (1–2), 231–243.
Tanaka, H., Ohta, T., Hiyama, T., Maximov, T.C., 2000. Seasonal variation of photosynthesis and transpiration properties of a boreal deciduous forest: analysis using a single layer canopy model. J. Jpn. For. Soc. 82 (3), 259–267.
Tang, R.L., Li, Z.L., Tang, B.H., 2010. An application of the Ts-VI triangle method with enhanced edges determination for evapotranspiration estimation from MODIS data in arid and semi-arid regions: implementation and validation. Remote Sens. Environ. 114 (3), 540–551.
Tittebrand, A., Schwieben, A., Berger, F., 2005. The influence of land surface parameters on energy flux densities derived from remote sensing data. Meteorol. Z. 14 (2), 227–236.
Tucker, C.J., Pinzon, J.E., Brown, M.E., Slayback, D.A., Pak, E.W., Mahoney, R., Vermote, E.F., Saleous, N.E., 2005. An extended AVHRR 8-km NDVI dataset compatible

with MODIS and SPOT vegetation NDVI data. Int. J. Remote Sens. 26 (20), 4485–4498.
Twine, T.E., Kustas, W.P., Norman, J.M., Cook, D.R., Houser, P.R., Meyers, T.P., Prueger, J.J., Starks, P.J., Wesely, M.L., 2000. Correcting eddy-covariance flux underestimates over a grassland. Agric. For. Meteorol. 103, 279–300.
Wang, K.C., Liang, S.L., 2008. An improved method for estimating global evapotranspiration based on satellite determination of surface net radiation, vegetation index, temperature, and soil moisture. J. Hydrometeorol. 9 (4), 712–727.
Wang, K.C., Li, Z., Cribb, M., 2006. Estimation of evaporative fraction from a combination of day and night land surface temperature and NDVI: a new method to determine the Priestley–Taylor parameter. Remote Sens. Environ. 102 (3–4), 293–305.
Wang, K.C., Wang, P.C., Li, Z.Q., Cribb, M., Sparrow, M., 2007. A simple method to estimate actual evapotranspiration from a combination of net radiation, vegetation index, and temperature. J. Geophys. Res. 112, D15107.
White, W.B., McKeon, G., Syktus, J., 2003. Australian drought: the interference of multi-spectral global standing modes and travelling waves. Int. J. Climatol. 23 (6), 631–662.
Wood, E.F., Lettenmaier, D.P., Zartarian, V.G., 1992. A land-surface hydrology parameterization with subgrid variability for general circulation models. J. Geophys. Res. 97 (D3), 2717–2728.
Yao, Y.J., Liang, S.L., Qin, Q.M., Wang, K.C., 2010. Monitoring drought over the conterminous United States using MODIS and NCEP Reanalysis-2 Data. J. Appl. Meteorol. Climatol. 49 (8), 1665–1680.
Zhang, R.H., Sun, X.M., Zhu, Z.L., Su, H.B., Tang, X.Z., 2003. A remote sensing model for monitoring soil evaporation based on thermal inertia and its validation. Sci. China Ser. D 46 (4), 342–355.
Zhang, Y.Q., Chiew, F.H.S., Zhang, L., Leuning, R., Cleugh, H.A., 2008. Estimating catchment evaporation and runoff using MODIS leaf area index and the Penman–Monteith equation. Water Resour. Res. 44 (10), W10420.
Zhao, M.S., Running, S.W., 2010. Drought-induced reduction in global terrestrial net primary production from 2000 through 2009. Science 329 (5994), 940–943.
Zhou, L.M., Dickinson, R.E., Tian, Y.H., Fang, J.Y., Li, Q.X., Kaufmann, R.K., Tucker, C.J., Myneni, R.B., 2004. Evidence for a significant urbanization effect on climate in china. PNAS 101 (26), 9540–9544.

Please cite this article in press as: Yao, Y., et al., Monitoring global land surface drought based on a hybrid evapotranspiration model. Int. J. Appl. Earth Observ. Geoinf. (2010), doi:10.1016/j.jag.2010.09.009